

**Broadband negative refraction in stacked fishnet metamaterial**

Zeyong Wei,<sup>1</sup> Yang Cao,<sup>1</sup> Jin Han,<sup>1</sup> Chao Wu,<sup>1</sup> Yuancheng Fan,<sup>1</sup> and Hongqiang Li<sup>1, a)</sup>

*Department of Physics, Tongji University, Shanghai 200092,  
China*

We demonstrate a scheme to utilize the stacked fishnet metamaterial for all-angle negative refraction and subwavelength imaging within a wide frequency range starting from zero frequency. The theoretical predictions are verified by the brute-force finite-difference-in-time-domain (FDTD) numerical simulations. The phenomena come from the negative evanescent coupling between the adjacent slab waveguides through the breathing air holes perforated on metal layers.

---

<sup>a)</sup>Electronic mail: hqlee@tongji.edu.cn

Since J.B. Pendry proposed perfect lens<sup>1</sup> using left-handed materials<sup>2</sup>, sustained attentions have been drawn to the negative-index metamaterial (NIM) with simultaneously negative permittivity and permeability. The NIM, comprising of subwavelength metallic resonant units, has been designed and realized in both the microwave<sup>3</sup> and optical regime<sup>4</sup>. Negative refraction and subwavelength imaging with NIMs have great application potentials in photonic devices<sup>5–10</sup>. Among various types of NIMs, one most promising candidate is the so-called fishnet NIM which comprises of alternating metal/dielectric layers perforated with two-dimensional array of holes<sup>11–15</sup>. The simple structure also provides a feasible solution for optical NIM<sup>16–21</sup>.

In the previous studies on the fishnet NIMs<sup>11–21</sup>, the light waves are incident on the top interface of the metal/dielectric multi-layers. Below the cut-off frequency of air holes the light waves can not penetrate into the structure and the negative index was retrieved within in a narrow frequency range above the cut-off. In this paper, a different incidence configuration is employed by impinging the light waves on the sidewall interface of fishnet NIM that is perpendicular to the metal/dielectric multi-layers. As the uniformly spaced holey metallic layers constitute a multiple of slab waveguides filled dielectric spacer layers, the incidence configuration of this kind enables us to fully exploit the optical properties of the fishnet NIM in the long wavelength limit. We show that the evanescent coupling between the slab waveguides gives rise to all-angle negative refraction and subwavelength imaging in a wide frequency range starting from zero frequency.

Figure 1 schematically illustrates the structure of our stacked fishnet metamaterial and the incidence configuration. The metal/dielectric layers are lying in  $\hat{x}\hat{y}$  plane. The square arrays of air holes perforated on metallic layers are aligned along  $z$  axis without lateral displacement in  $\hat{x}\hat{y}$  plane. The period of the hole array, the thickness of metallic layer and dielectric layer are  $p = 6.0\text{mm}$ ,  $t = 0.035\text{mm}$  and  $h = 1.575\text{mm}$  respectively. The line width of metallic strips along  $x$  direction  $w = 0.2\text{mm}$  is the same as that along  $\hat{y}$  direction, and the size of square holes is  $a = p - g = 5.8\text{mm}$ . The dielectric constant of the dielectric layer is  $\epsilon_r = 2.2$ . The EM incidence waves are propagating in the  $\hat{x}\hat{z}$  plane with an incident angle of  $\theta$ . Under the assumption of perfectly electric conductor (PEC) for metals, the electromagnetic fields in the region of holey metallic layers, only existing in the air holes, shall be accurately expressed as the superposition of local modes guided in square holes; while the waves inside a dielectric spacer layer shall be expressed with the expansion of

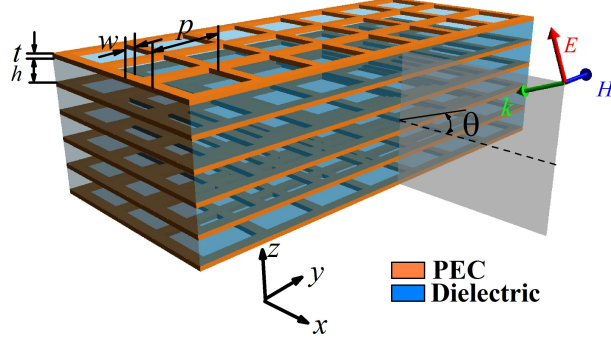


FIG. 1. The schematic of stacked fishnet metamaterial. The red and blue arrows indicate the directions of electric field  $\vec{E}$  and magnetic field  $\vec{H}$  of incident waves. The plane in gray color denotes the incident plane.

guided Bloch waves in terms of periodicity in xy plane. By applying the boundary continuity conditions at the interfaces of metal/dielectric layers (over the air holes) and the periodic boundary condition along z direction for tangential components of both the electric and magnetic fields, we can rigorously resolve the dispersion relation of the three-dimensional stacked structure by the modal expansion method<sup>22–25</sup>. At wavelengths much longer than both the thickness  $h$  of dielectric layer and the size  $a$  of square hole, the calculations are quickly convergent with just one or a few more local modes considered in hole waveguide.

Figure 2 presents the calculated dispersion diagram along the  $\Gamma(0,0,0) \rightarrow X(0.5,0,0)$ ,

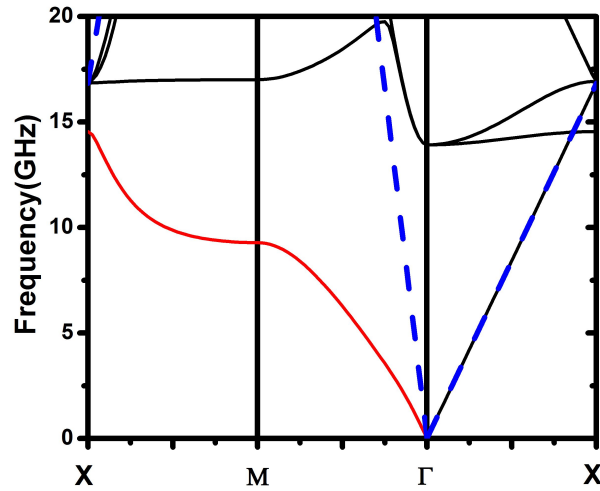


FIG. 2. Dispersion diagram of the stacked fishnet metamaterial along  $\Gamma(0,0,0) \rightarrow X(0.5,0,0)$ ,  $\Gamma(0,0,0) \rightarrow M(0.5,0,0.5)$  and  $M(0.5,0,0.5) \rightarrow X(0.5,0,0)$  directions.

$\Gamma(0,0,0) \rightarrow M(0.5,0,0.5)$  and  $M(0.5,0,0.5) \rightarrow X(0.5,0,0)$  directions. The blue dashed line refers to the light line in the dielectric. We notice that, the lowest branch along the  $\Gamma X$  direction ( $k_z = 0$ ) precisely coincides with the light line. This is understandable with the help of modal expansion method. Detailed calculations show that these  $k_z = 0$  states only contain the  $0^{th}$  order Bloch component which is the transverse electromagnetic (TEM) mode that is always orthogonal to the local modes of air hole. In this situation, the free photons in the dielectric are the only choice for the  $k_z = 0$  states as no evanescent couplings happen via the breathing air holes. However the lowest branch ( $k_z \neq 0$ ) along the  $\Gamma M$  and  $XM$  directions (red solid line in Fig.2) evidently deviates from the light line in dielectric. The  $k_z \neq 0$  states on this branch originate from the evanescent coupling between the adjacent slab waveguides via the  $TE_{10}$  mode of holes (noting that the overlap integral between a high order of guided Bloch mode and local mode of air hole is not zero). Figure 3(a) presents the charts of equi-frequency surface (EFS) analysis for the  $k_y = 0$  states to further reveal the characteristics of this band. All curves in Fig. 3(a) are in a hyperbolic-like line shape, which indicates that broadband all-angle negative refraction occurs in the  $\hat{x}\hat{z}$  plane below the cutoff frequency of air holes. At lower frequency the curves in Fig. 3(a) become much more flat, which means that the waves are also strongly collimated inside the structure along the direction parallel to the metal/dielectric layers. A numerical proof of negative refraction is shown in Fig. 3(b). In our FDTD simulations, a monochromatic one-way Gaussian beam in the  $\hat{x}\hat{z}$  plane with a frequency at 11GHz is incident at an incident angle of  $30^\circ$ . The fishnet model is stacked by 500 metal/dielectric layers along  $z$  direction. Given the periodicity of hole arrays and the incidence configuration, 60 periods along  $x$  direction and one period along  $y$  direction are adopted for the metal/dielectric layers in the model. The negative refraction is clearly shown in Fig. 3(b) with the magnetic field distribution in the  $\hat{x}\hat{z}$  plane. The black arrows denote the directions of energy flow in the free space and fishnet structure. A refraction angle of  $-16.2^\circ$ , retrieved from the refracted direction of the energy flow in the metamaterial or the negative Goos-Hanchen shift alternatively, is in good agreement with the estimate by EFS analysis. We also see from Fig. 3(b) that the beam can easily propagate inside the structure without any reflection.

The optical properties of such a system can be described with the coupled wave equation<sup>26–28</sup> by considering the coupling between the  $n^{th}$  waveguide channel and its nearest

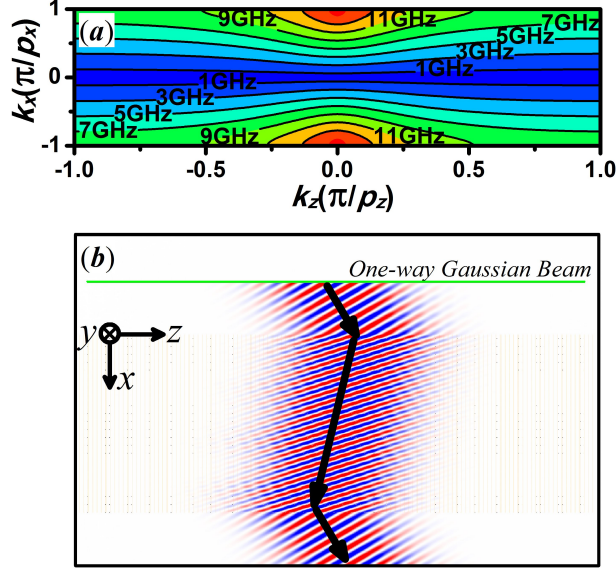


FIG. 3. (a) The charts of EFS analysis for the lowest branch at  $k_y=0$ . (b) The distribution of magnetic field ( $H_y$ ) in the  $\hat{x}\hat{z}$  plane calculated by the FDTD simulations. The green line denotes the position of the one-way Gaussian beam about 70mm away from the top interface of our fishnet model.

neighbors, the  $(n-1)^{th}$ ,  $(n+1)^{th}$  waveguide channels, as:

$$i\frac{da_n(x)}{dx} + \beta a_n(x) + C[a_{n+1}(x) + a_{n-1}(x)] = 0 \quad (1)$$

Where  $a_n(x)$  denotes the wave fields in the  $n^{th}$  slab waveguide,  $C$  is the coupling coefficient, and  $\beta$  is the propagation constant of free photons in the dielectric. Under the periodic boundary condition along  $z$  direction, the dispersion of the system takes the form as

$$k_x = \beta + 2C \cos(k_z p) \quad (2)$$

where  $k_x$  and  $k_z$  are the vector components along the  $x$  and  $z$  directions. At  $k_z = 0$ , the coupling coefficient  $C = 0$  is zero (as aforementioned no evanescent coupling occurs) and we have  $k_x = \beta$  which is rightly the light line in the dielectric. While at  $k_z \neq 0$ , the coupling coefficient  $C$  is always negative in the limit of long wavelength (which can be deduced from the charts in Fig. 3(a)), giving rise to all-angle negative refraction. We note that the silver/dielectric multi-layered structure also supports all-angle negative refraction in a certain optical frequency regime under the same incidence configuration of our study<sup>29</sup>. The long range SPPs play an important role for the negative refraction. We also note that,

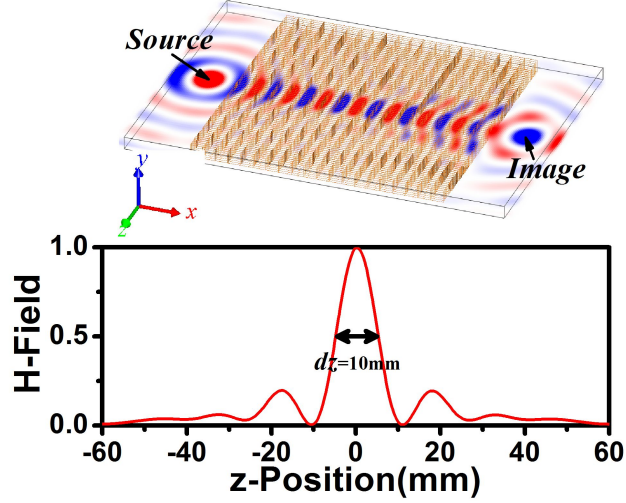


FIG. 4. (a) The snap shot of magnetic field distribution in the incident plane. The model, stacked by 80 metal/dielectric multi-layers along  $z$  axis, has 20 periods along  $\hat{x}$  direction and one period along  $\hat{y}$  direction. (b) Normalized magnetic field profile at the image plane as a function of  $z$  coordinate.

at long wavelength limit, a holey metallic surface can be homogenized into a single-negative medium with electric response in the form of Drude model<sup>30</sup>. The plasmon frequency is rightly the cut-off frequency of air holes. Thus it is reasonable for us to consider the stacked fishnet metamaterial as an artificial plasmonic waveguide array. The negative coefficient  $C$  implies that for the eigenstates on the lowest branch, the spatial field distributions are anti-symmetric with respect to the plane of air holes. If our findings are applicable in the optical regime where metals are dispersive and dissipative, the most field energy shall propagate outside the lossy metal film with anti-symmetric field distribution, and low loss is expected. The picture may be helpful to explain the low loss measured in a recent experiment about fishnet optical NIMs<sup>16,19</sup>.

One important application of all-angle negative refraction is flat lens. The imaging performance of our stacked fishnet metamaterial is examined by the brute-force FDTD numerical simulations. As shown in Fig. 4(a), a monochromatic line source with a frequency at 11GHz is positioned 15mm away from the surface at the left side of the fishnet structure. The snap shot shown in Fig. 4(a) clearly indicates a high-quality image achieved at the image plane—about 15mm away from the outgoing interface at the other side. The image resolution can be checked by the normalized magnetic field profile at image plane. As illustrated in Fig.

4(b), along  $\hat{z}$  axis, the full width at half maximum (FWHM) of the field profile is 10mm about one-third of the wavelength. The FWHM at a lower frequency still remains at about 10mm, leading to a better resolution in subwavelength scale along the  $\hat{z}$  direction. But a longer structure along x direction is required due to stronger collimation effect at lower frequency. Further simulations indicate that the subwavelength imaging can be achieved in far-field (not shown).

In conclusion, the fishnet metamaterials can operate as plasmonic waveguide arrays. Our findings about the broadband negative refraction and subwavelength imaging in the long wavelength limit have great potentials for photonic devices in microwave, THz and even in the optical regimes. This work was supported by NSFC (No. 10974144, 60674778), the National 863 Program of China (No. 2006AA03Z407), NCET (07-0621), STCSM and SHEDF (No. 06SG24).

## REFERENCES

- <sup>1</sup>J. B. Pendry, Phys. Rev. Lett. **85**, 3966 (2000).
- <sup>2</sup>V. G. Veselago, Sov. Phys. Usp. **10**, 509 (1968).
- <sup>3</sup>R. A. Shelby, D. R. Smith, and S. Schultz, Science **292**, 77 (2001).
- <sup>4</sup>N. Liu, H. C. Guo, L. W. Fu, S. Kaiser, H. Schweizer, and H. Giessen, Nat. Mater. **7**, 31 (2008).
- <sup>5</sup>A. Grbic and G. Eleftheriades, Phys. Rev. Lett. **92**, 117403 (2004).
- <sup>6</sup>M. Wiltshire, J. Pendry, and J. Hajnal, J. Phys.: Condens. Matter **18**, L315 (2006).
- <sup>7</sup>P. Belov, Y. Hao, and S. Sudhakaran, Phys. Rev. B **73**, 033108 (2006).
- <sup>8</sup>M. Freire, R. Marques, and L. Jelinek, Appl. Phys. Lett. **93**, 231108 (2008).
- <sup>9</sup>M. Silveirinha, C. Fernandes, and J. Costa, Phys. Rev. B **78**, 195121 (2008).
- <sup>10</sup>M. Silveirinha, C. Medeiros, C. Fernandes, and J. Costa, Phys. Rev. B **81**, 033301 (2010).
- <sup>11</sup>M. Beruete, I. Campillo, J. E. Rodriguez-Seco, E. Perea, M. Navarro-Cia, I. J. Nunez-Manrique, and M. Sorolla, Ieee Microwave and Wireless Components Letters **17**, 831 (2007).
- <sup>12</sup>M. Beruete, M. Navarro-Cia, M. Sorolla, and I. Campillo, J. Appl. Phys. **103**, 053102 (2008).
- <sup>13</sup>M. Navarro-Cia, M. Beruete, M. Sorolla, and I. Campillo, Opt. Express **16**, 560 (2008).

- <sup>14</sup>M. Beruete, M. Sorolla, M. Navarro-Cia, F. Falcone, I. Campillo, and V. Lomakin, *Opt. Express* **15**, 1107 (2007).
- <sup>15</sup>M. Navarro-Cia, M. Beruete, M. Sorolla, and I. Campillo, *Appl. Phys. Lett.* **94**, 144107 (2009).
- <sup>16</sup>G. Dolling, C. Enkrich, M. Wegener, C. Soukoulis, and S. Linden, *Science* **312**, 892 (2006).
- <sup>17</sup>S. Zhang, W. Fan, N. Panoiu, K. Malloy, R. Osgood, and S. Brueck, *Opt. Express* **14**, 6778 (2006).
- <sup>18</sup>G. Dolling, M. Wegener, and S. Linden, *Opt. Lett.* **32**, 551 (2007).
- <sup>19</sup>J. Valentine, S. Zhang, T. Zentgraf, E. Ulin-Avila, D. Genov, G. Bartal, and X. Zhang, *Nature* **455**, 376 (2008).
- <sup>20</sup>Z. Ku and S. R. J. Brueck, *Appl. Phys. Lett.* **94**, 153107 (2009).
- <sup>21</sup>Z. Y. Ku, J. Y. Zhang, and S. R. J. Brueck, *Opt. Express* **17**, 6782 (2009).
- <sup>22</sup>P. Sheng, R. S. Stepleman, and P. N. Sanda, *Phys. Rev. B* **26**, 2907 (1982).
- <sup>23</sup>P. Lalanne, J. P. Hugonin, S. Astilean, M. Palamaru, and K. D. Moller, *J. Opt. a-Pure Appl. Op.* **2**, 48 (2000).
- <sup>24</sup>Z. Wei, J. Fu, Y. Cao, C. Wu, and H. Li, *Photonics Nanostruct.* **8**, 94 (2010).
- <sup>25</sup>Z. Wei, H. Li, C. Wu, Y. Cao, J. Ren, Z. Hang, H. Chen, D. Zhang, and C. Chan, *Opt. Express* **18**, 12119 (2010).
- <sup>26</sup>H. Haus and L. Molter-Orr, *Quantum Electronics, IEEE Journal of* **19**, 840 (1983).
- <sup>27</sup>H. Eisenberg, Y. Silberberg, R. Morandotti, and J. Aitchison, *Phys. Rev. Lett.* **85**, 1863 (2000).
- <sup>28</sup>T. Pertsch, T. Zentgraf, U. Peschel, A. Brauer, and F. Lederer, *Phys. Rev. Lett.* **88**, 093901 (2002).
- <sup>29</sup>J. B. Pendry, L. Martin-Moreno, and F. J. Garcia-Vidal, *Science* **305**, 847 (2004).
- <sup>30</sup>X. Fan, G. Wang, J. Lee, and C. T. Chan, *Phys. Rev. Lett.* **97**, 073901 (2006).